Approximate Performance of Periodic Hypersonic Cruise Trajectories for Global Reach

Preston H. Carter II*
Lawrence Livermore National Laboratory, Livermore, California 94550
and
Darryll J. Pines† and Lael vonEggers Rudd‡
University of Maryland, College Park, Maryland 20742

This paper develops the analytical framework to compare the approximate performance of periodic hypersonic cruise trajectories with previously proposed hypersonic trajectory profiles for global reach. Specifically, range, ΔV, and payload-carrying capacity are evaluated for various trajectory types to illustrate the enhanced performance achieved by flying periodic hypersonic cruise trajectories with existing hypersonic vehicle aerodynamic, propulsion, and structures technology. Analytical results reveal that periodic hypersonic cruise trajectories achieve better fuel-consumption savings and deliver more payload over long distances ($\approx 20{,}000$ km) than other trajectory types proposed for high-speed flight. Over 20% improvement in fuel consumption savings is possible for a Mach 10 vehicle with a modest L/D of 4, and a curve-fitted rocket-based combined cycle engine model.

Nomenclature

A	=	area
A	=	vector term
a	=	speed of sound
C_D	=	drag coefficient
C_L	=	lift coefficient
c	=	exhaust velocity
D	=	drag
E	=	range/mass parameter
F	=	force vector
h	=	height
h_{scale}	=	atmospheric scale height
I_{sp}	=	specific impulse
I_{sp}^e	=	effective specific impulse
L	=	lift
MF	=	vehicle fuel mass fraction
MR	=	mass fraction
m	=	mass
m_e	=	mass of engine
m_f	=	mass of fuel
m_P	=	mass of payload
m_s	=	mass of structure
n	=	number of periods
R	=	range
R_e	=	radius of the Earth
s	=	length
T	=	thrust vector
t	=	time
V	=	velocity
$\bar{V}$	=	dimensionless velocity
$\hat{v}$	=	velocity unit vector
β_{C_L}	=	ballistic coefficient
γ	=	flight-path angle
ε	=	fuel weight fraction
π	=	natural number
ρ	=	density
ρ_f	=	reference density
ϕ	=	nondimensional range

Subscripts

A	=	aerodynamic
a	=	aerodynamic
en	=	entrance
ex	=	exit
f	=	final
I	=	impulsive
i	=	initial
0	=	conditions after powered flight

Introduction

IN the past four decades there has been a considerable amount of interest in developing hypersonic vehicles for a host of applications. Initial interest in such vehicles originated from post-World War II military requirements to develop a long-range, high-speed weapons delivery system that could strike an adversary more than halfway ($\approx 20{,}000$ km) around the world. Modern interest in hypersonic flight has been motivated by the potential for long-range intercontinental transport, involving both cargo and persons. In addition, because the basic requirements of a hypersonic vehicle are similar to orbital launch vehicles, modern interest has been in reusable transatmospheric vehicles that can fly to and from Earth orbit using the same technology as a hypersonic airplane.

Trajectory Types

A variety of trajectories has been proposed and studied to address high-speed flight across intercontinental distances. These trajectory forms include 1) steady-state cruising trajectories at subsonic, supersonic, and hypersonic speeds; 2) suborbital ballistic trajectories; 3) boost-glide trajectories; and 4) skipping boost-glide trajectories. The practice of aerial refueling has also been used to extend the performance of subsonic and supersonic aircraft.

Currently, most applications for long-range and high-speed flight are limited to using subsonic cruising trajectories, and to a lesser extent, supersonic cruising trajectories. These trajec-

tories do not satisfy the need for fast long-range transportation. Many proposed applications that require intercontinental trip times of a few hours are not possible or practical with the current state of the art in aerospace technology. Therefore, a trajectory that could provide high-speed transportation between intercontinental distances in a matter of hours without significant advances in the current state of the art of aerospace technologies in aerodynamics, propulsion, or structures would be of considerable interest to the civilian and military sectors.

Periodic Hypersonic Cruise Trajectories

The discovery of periodic cruise trajectories for hypersonic flight has evolved from extensive analytical and computational optimization studies to determine possible trajectory types that could achieve better fuel-consumption savings. With this goal in mind, several researchers have found suboptimal and optimal periodic cruise trajectories that achieve better fuel-consumption savings between two destinations over steady-state cruise. However, these numerically computed solutions are sensitive to initial and final boundary conditions as well as vehicle propulsion technology and configuration. Nevertheless, computational optimization results indicate that fuel-consumption savings of 8–45% are possible over a single period.[1-5] However, it is difficult to compare these optimal solutions because many are computed using different vehicle and propulsion models. This paper attempts to develop a consistent approximate analytical framework for the purpose of comparing various trajectory types for long-range.

Periodic hypersonic cruise (PHC) trajectories use a skipping or re-entry trajectory with propulsion impulses to sustain the skipping motion to achieve the desired range. As a skipping trajectory, the vehicle follows a flight path that uses the Earth's atmosphere in a manner similar to a rock skipping across the

surface of a lake. At high speed, a lifting body or waverider class vehicle will skip in and out of the atmosphere because of lightly damped phugoid oscillation. This skipping can be continued indefinitely by thrusting at the low point of the trajectory to make up for losses caused by aerodynamic drag. Figure 1 displays an exaggerated comparison of a PHC trajectory to subsonic cruise (SUBC), supersonic and hypersonic cruise (HC), hypersonic boost-glide (HBG), and suborbital ballistic (SUBO) trajectories.

The flight profile is divided into four major phases: boost, periodic cruise, glide, and landing. During the boost phase, the vehicle is accelerated to the desired altitude and velocity for beginning a skipping trajectory. Ideally, to maximize the range for a given amount of fuel, the boost velocity, V_0, should be as high as possible. In reality, the initial boost velocity is limited by the current state of air-breathing or rocket-propulsion technology. The selected boost velocity will reflect a tradeoff between trajectory performance and available propulsion technology.

During the cruise phase the vehicle is engaged in its skipping motion, sustained with impulsive propulsion burns to maintain the mean altitude of the skipping motion. The sustaining burns are performed during each passage through the atmosphere to make up for energy lost because of aerodynamic drag. Cruise continues until all of the fuel is expended.

The glide phase begins when the sustaining burns are discontinued. After the sustaining burns are discontinued, skipping motion gives way to steady glide with both altitude and velocity decreasing. This entire phase is most likely unpowered. At the terminal end of this phase the vehicle lands. The landing can be powered or unpowered.

Performance Analysis

The performance of a PHC trajectory can be analyzed by evaluating the contributions of each phase separately (Fig. 2). By computing the approximate range and ΔV requirements for each of these phases, one can compare analytically the performance of periodic cruise trajectories to other trajectory types for long-range. The analysis for conducting such a performance study is developed next for each phase of the periodic trajectory.

In this study the following assumptions are made.

1) Flight occurs in one plane corresponding to a great circle between takeoff and landing.

2) Aerodynamic heating is neglected.

3) G-forces are also negelected.

4) Sufficient guidance, navigation, and control are available to fly the vehicle along periodic hypersonic cruise trajectories.

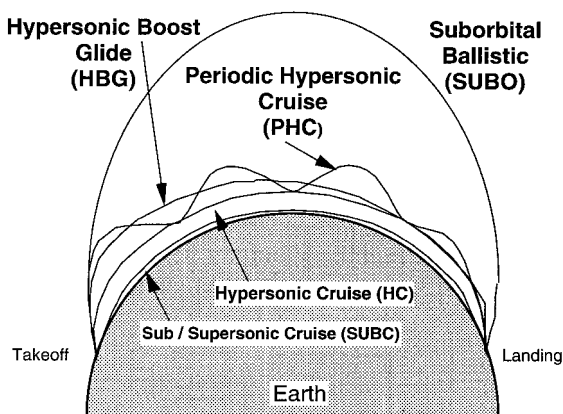5) Atmosphere is isothermal (constant speed of sound of 300 m/s).
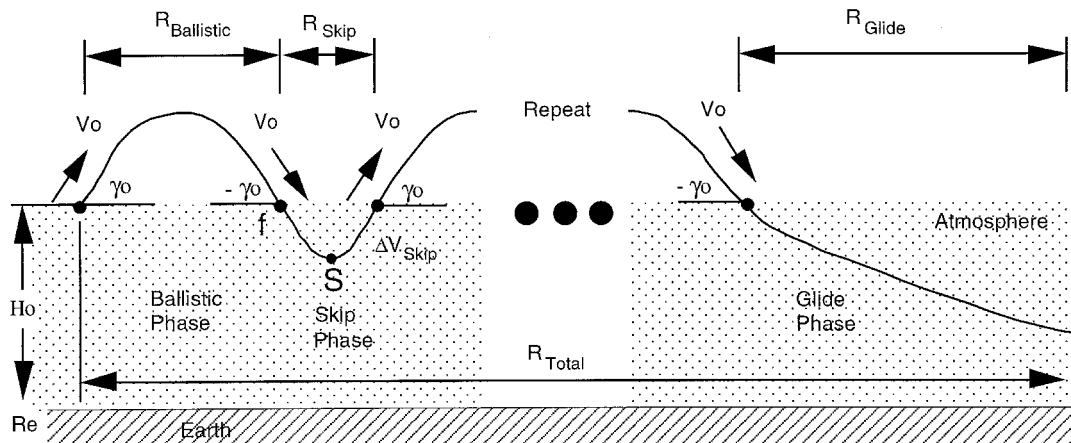

Fig. 1   Comparison of trajectory shapes.

Fig. 2   Parameters of a periodic hypersonic cruise trajectory.

Range Approximation

Taking the preceding assumptions into account, the total range of a periodic hypersonic cruise trajectory (Fig. 2) can be estimated by summing the individual contributions of each phase

$$R_{\text{Total}} = R_{\text{Boost}} + nR_{\text{Ballistic}} + (n-1)R_{\text{Skip}} + R_{\text{Glide}} \qquad (1)$$

where R corresponds to the range of the various phases, and n is the number of periods used in the flight. Assuming that the range associated with the boost phase is negligible, i.e., $R_{\text{Boost}} = 0$, the total range equation can be rewritten as

$$R_{\text{Total}} = nR_{\text{Ballistic}} + (n-1)R_{\text{Skip}} + R_{\text{Glide}} \qquad (2)$$

The nondimensional form of the total range equation can be computed by dividing through by $2\pi R_e$. Thus, Eq. (2) in nondimensional form becomes

$$\phi_{\text{Total}} = R_{\text{Total}}/2\pi R_e \qquad (3)$$

Ballistic

After traveling through the accelerated boost phase to get up to altitude, the hypersonic vehicle's trajectory is approximated as following a ballistic arc as the vehicle exits the atmosphere to initiate the first leg of periodic cruise. The approximate range for this ballistic arc was first developed by Sanger and Brendt,[6] and was later refined by Eggers et al.[7] Assuming a keplerian formulation of the vehicle dynamics, Eggers et al. determined that the ballistic range could be approximated as

$$\phi_{\text{Ballistic}} = \frac{R_{\text{Ballistic}}}{2\pi R_e} = \frac{1}{\pi} \arctan \frac{\sin \gamma_f \cos \gamma_f}{(1/V_f^2) - \cos^2\gamma_f} \qquad (4)$$

where ϕ is the total angle of arc traveled around the Earth, $R_{\text{Ballistic}}$ is the actual ballistic range traveled, $\gamma_f = -\gamma_0$ is the flight-path angle at the end of boost, $\bar{V}_f = V_0/V_s$ is the nondimensional velocity at the end of powered flight, V_0 is the boost velocity, and V_s is the orbital velocity at sea level.

Skip

As the vehicle re-enters the Earth's atmosphere after traversing the ballistic arc, it will be subjected to aerodynamic lift and drag forces that will cause it to undergo a skipping trajectory. The range of this skipping trajectory can be determined by accounting for the effects of lift and drag through an isothermal atmosphere. The following range calculation assumes that the skip exit velocity is the same as the skip entrance velocity.

Consider the vertical component of the equation of motion for a vehicle in the atmosphere

$$\tfrac{1}{2}\rho V^2/\beta_{C_L} - g \cos \gamma = -[V^2\cos^2\gamma/(R_e + h)] \qquad (5)$$

where β_{C_L} is the ballistic coefficient for lift given by

$$\beta_{C_L} = m/C_L A \qquad (6)$$

Assuming that $R_e + h$ is approximately equal to R_e, Eq. (5) can be solved for the density ρ, and written as

$$\rho = (2\beta_{C_L}/V^2)[g \cos \gamma - (V^2\cos^2\gamma/R_e)] \qquad (7)$$

Any point in the skip maneuver may be compared with the initial point f (Fig. 2) by the skip re-entry equation of motion[8]

$$\cos \gamma - \cos \gamma_f = (h_{\text{scale}}/2\beta_{C_L})(\rho - \rho_f) \qquad (8)$$

where h_{scale} is the atmospheric scale height constant for an exponential model of the atmosphere, given by

$$\rho/\rho_f = \exp(-y/h_{\text{scale}}) \qquad (9)$$

where $y = h - h_f$. At the lowest point in the skip maneuver, defined as point s (Fig. 2), $\gamma_s = 0$. Therefore, Eq. (8) becomes

$$(1 - \cos \gamma_f) = (h_{\text{scale}}/2\beta_{C_L})(\rho_s - \rho_f) \qquad (10)$$

Substituting Eq. (7) into Eq. (10) yields

$$(1 - \cos \gamma_f) = (h_{\text{scale}}\rho_s/2\beta_{C_L}) - (h_{\text{scale}}/V_0^2)g' \qquad (11)$$

where

$$g' = [g \cos \gamma_f - (V_0^2 \cos^2\gamma_f/R_e)] \qquad (12)$$

Substituting for the density at point s, into Eq. (11), leads to

$$\exp(-y/h_{\text{scale}}) - 1 = \frac{V_0^2(1 - \cos \gamma_f)}{h_{\text{scale}}g'} \qquad (13)$$

Solving for y results in

$$y = h_s - h_f = -h_{\text{scale}} \ell n \left[1 + \frac{V_0^2(1 - \cos \gamma_f)}{h_{\text{scale}}g'} \right] \qquad (14)$$

where $h_f = h_s - y$. Equation (14) is an estimate of the maximum depth that the vehicle reaches during the skip phase. This is similar to the common ballistic re-entry problem. If it is assumed that

$$[(h_s - h_f)/(R_s - R_f)] = \tan \gamma_f \qquad (15)$$

where R_s and R_f are horizontal ranges, then the approximate skip range is given by

$$R_{\text{Skip}} = 2(R_s - R_f) = 2[(h_s - h_f)/\tan \gamma_f] \qquad (16)$$

so that the nondimensional skip range is given by

$$\phi_{\text{Skip}} = \frac{R_{\text{Skip}}}{2\pi R_e} = \frac{1}{\pi R_e} \left(\frac{-h_{\text{scale}} \ell n\{1 + [V_0^2(1 - \cos \gamma_f)/h_{\text{scale}}g']\}}{\tan \gamma_f} \right) \qquad (17)$$

Glide

Once the sustained skip phase is terminated, the vehicle is capable of gliding the remaining distance to reach its final destination. To account for this additional range, Eggers et al.[7] derived the following range equation for the glide portion of flight:

$$\phi_{\text{Glide}} = \frac{R_{\text{Glide}}}{2\pi R_e} = \frac{1}{4\pi} \left(\frac{L}{D} \right) \ell n \left(\frac{1}{1 - \bar{V}_f^2} \right) \qquad (18)$$

Summing the contribution from each phase, the total nondimensional range for a PHC flight becomes

$$\phi_{\text{Total}} = n\phi_{\text{Ballistic}} + (n-1)\phi_{\text{Skip}} + \phi_{\text{Glide}} \qquad (19)$$

Substituting the range for each phase leads to

$$\phi_{\text{Total}} = n \left[\frac{1}{\pi} \arctan \frac{\sin \gamma_f \cos \gamma_f}{(1/\bar{V}_f^2) - \cos^2\gamma_f} \right] + (n-1) \frac{1}{\pi R_e}$$
$$\times \left(\frac{-h_{\text{scale}} \ell n\{1 + [V_0^2(1 - \cos \gamma_f)/h_{\text{scale}}g']\}}{\tan \gamma_f} \right)$$
$$+ \frac{1}{4\pi} \left(\frac{L}{D} \right) \ell n \left(\frac{1}{1 - \bar{V}_f^2} \right) \qquad (20)$$

ΔV Approximation

The fuel consumption for PHC trajectories can be determined by accounting for how much ΔV is expended during each phase of the cycle. Recall that PHC trajectories are achieved by first boosting up to altitude and then sustaining the periodicity with successive burns during the skip phases. Thus, the total ΔV can be represented as

$$\Delta V_{\text{Total}} = \Delta V_{\text{Boost}} + (n - 1)\Delta V_{\text{Skip}} \tag{21}$$

Boost

Because the boost phase may be achieved with a variety of propulsion technologies, including rocket, airbreathing, or a combination of the two, such as rocket-based combined cycle (RBCC) engine technology, a generic scheme for estimating the impulsive ΔV during this phase is required.

Consider the vector equation of motion of a boosting or accelerating hypersonic vehicle given by

$$\frac{\mathrm{d}\boldsymbol{V}}{\mathrm{d}t} = \frac{\boldsymbol{T}}{m} + \frac{\boldsymbol{F}_a}{m} - \boldsymbol{g} \tag{22}$$

where $\boldsymbol{T}$, $\boldsymbol{F}_a$, and $\boldsymbol{g}$ represent the thrust, aerodynamic, and gravitational forces acting on the vehicle, respectively. Define the term, $\boldsymbol{A}$, to be given by

$$\boldsymbol{A} = (\boldsymbol{F}_a/m) - \boldsymbol{g} \tag{23}$$

The thrust, $\boldsymbol{T}$, is given by

$$\boldsymbol{T} = -\boldsymbol{c}\,\frac{\mathrm{d}m}{\mathrm{d}t} \tag{24}$$

where $\boldsymbol{c}$ is a vector thrust coefficient, and $\mathrm{d}m/\mathrm{d}t$ accounts for mass lost from the vehicle. Substituting Eqs. (23) and (24) into Eq. (22) leads to

$$\frac{\mathrm{d}\boldsymbol{V}}{\mathrm{d}t} = -\frac{\boldsymbol{c}}{m}\frac{\mathrm{d}m}{\mathrm{d}t} + \boldsymbol{A} \tag{25}$$

Multiplying through by $\mathrm{d}t$ leads to the following expression for the change in the vehicle velocity vector, $\boldsymbol{V}$:

$$\mathrm{d}\boldsymbol{V} = -\boldsymbol{c}\,\frac{\mathrm{d}m}{m} + \boldsymbol{A}\,\mathrm{d}t \tag{26}$$

Assuming that the direction of the thrust opposes the velocity vector, Eq. (26) can be rewritten as

$$\boldsymbol{T} = c\hat{\boldsymbol{v}}\,\frac{\mathrm{d}m}{\mathrm{d}t} \tag{27}$$

where $\hat{\boldsymbol{v}}$ is a unit vector whose magnitude is 1. Rewriting $\boldsymbol{V}$ as

$$\boldsymbol{V} = V\hat{\boldsymbol{v}} \tag{28}$$

Equation (26) can be rewritten as

$$\mathrm{d}\boldsymbol{V} = \mathrm{d}V\hat{\boldsymbol{v}} + V\,\mathrm{d}\hat{\boldsymbol{v}} = -c\,\frac{\mathrm{d}m}{\mathrm{d}t}\,\hat{\boldsymbol{v}} + (\boldsymbol{A}\,\mathrm{d}\cdot\hat{\boldsymbol{v}} + \boldsymbol{A}\cdot\hat{\boldsymbol{v}})\,\mathrm{d}t \tag{29}$$

Collecting the $\hat{\boldsymbol{v}}$ components and solving for the change in the velocity magnitude leads to

$$\mathrm{d}V = -c\,\frac{\mathrm{d}m}{m} + \boldsymbol{A}\cdot\hat{\boldsymbol{v}}\,\mathrm{d}t \tag{30}$$

Now let

$$\mathrm{d}V = \mathrm{d}V_I + \mathrm{d}V_A \tag{31}$$

where the impulsive (I) and aerodynamic (A) contributions to ΔV are given by

$$\mathrm{d}V_I = -c\,\frac{\mathrm{d}m}{m} \tag{32}$$

$$\mathrm{d}V_A = |\boldsymbol{A}\cdot\hat{\boldsymbol{v}}|\,\mathrm{d}t \tag{33}$$

From the examination of typical boosting trajectories,[9] a rough approximation of the relationship between $\mathrm{d}V$ and $\mathrm{d}V_I$ can be developed. Assume that a function, $f(V)$, relates the total ΔV to the impulsive $\mathrm{d}V_I$ through the equation

$$\mathrm{d}V = f(V)\,\mathrm{d}V_I \tag{34}$$

where $f(V) \geq 1$. Using the approximation function, $f(V)$, $\mathrm{d}V_A$ and $\mathrm{d}V_I$ become

$$\mathrm{d}V_A = \frac{f(V) - 1}{f(V)}\,\mathrm{d}V \tag{35}$$

$$\mathrm{d}V_I = \frac{\mathrm{d}V}{f(V)} \tag{36}$$

From this formulation the approximate impulsive ΔV_I for the boost phase can be estimated by integrating Eq. (36) over the velocity range of interest to obtain the generalized formula

$$\Delta V_I = \int_{V_i}^{V_o} \frac{1}{f(V)}\,\mathrm{d}V \tag{37}$$

This equation holds for a variety of propulsion technologies. For the current boost-phase analysis, the function $f(V)$ is derived from an ascent profile of a single-stage-to-orbit vehicle.[9] The function approximation for this system is given by

$$f(V) = 1 - \exp(-7.687 \times 10^{-4}\,V - 0.400) \tag{38}$$

Substituting Eq. (38) into Eq. (37) and integrating leads to the following formula representing the impulsive ΔV for the boost phase of all high-speed trajectory types:

$$\begin{aligned}\Delta V_{\text{Boost}} = \Delta V_I =&\ \frac{\ell n\,|\exp(-7.687 \times 10^{-4}\,V_o - 0.400) - 1|}{7.687 \times 10^{-4}} \\ &- \frac{\ell n\,|\exp(-7.687 \times 10^{-4}\,V_i - 0.400) - 1|}{7.687 \times 10^{-4}} + V_o - V_i\end{aligned} \tag{39}$$

The modeling of ΔV_{Boost} in this manner does not capture the details of an ascent trajectory in terms of impulse expended with respect to velocity gained. However, for boost velocities exceeding 2000 m/s, this is a good representation of the integrated effects of a typical ascent trajectory. Figure 3 shows a plot of ΔV_I vs V_o for a $V_i = 0$.

Skip

With the boost-phase ΔV approximated for typical hypersonic ascent profiles, it remains to estimate the ΔY during the successive skip phases used to sustain the PHC. During the skip phase the vehicle enters the atmosphere and is slowed by aerodynamic drag. The aerodynamic drag, according to Eggers et al.,[7] causes the velocity of the vehicle at the end of the skip

to be related to the velocity at the beginning through the following equation:

$$V_{ex_n}/V_{en_{n-1}} = \exp\{-[2\gamma_f/(L/D)]\} \qquad (40)$$

where V_{ex} is the exit velocity at the end of the skip, and $V_{en} = V_0$ is the entrance velocity at the beginning of the skip.

Without any propulsion burns during these skip phases, the vehicle's velocity after $(n - 1)$ skips would be

$$V_{end} = V_0 \exp\{-2(n - 1)[\gamma_f/(L/D)]\} \qquad (41)$$

To sustain the PHC trajectory, propulsive burns are required that return the exit velocity back to the original entrance velocity after each skip. This implies that for a single period the required ΔV is given by

$$\Delta V_{Skip} = V_0(1 - \exp\{-[2\gamma_f/(L/D)]\}) \qquad (42)$$

Summing the contributions of the boost and skip phases, the total ΔV required for a periodic hyersonic cruise trajectory is given by

$$\Delta V_{Total} = \Delta V_{Boost} + (n - 1)\Delta V_{Skip} \qquad (43)$$

Therefore, for a given boost velocity, V_0, there is an optimal γ_f that will produce a maximum $R_{Ballistic}/\Delta V_{Skip}$. A simple iterative method is used to search for this optimal γ_f using Eqs. (4) and (42). Figure 4 shows the ΔV_{Total} vs R_{Total}, assuming the
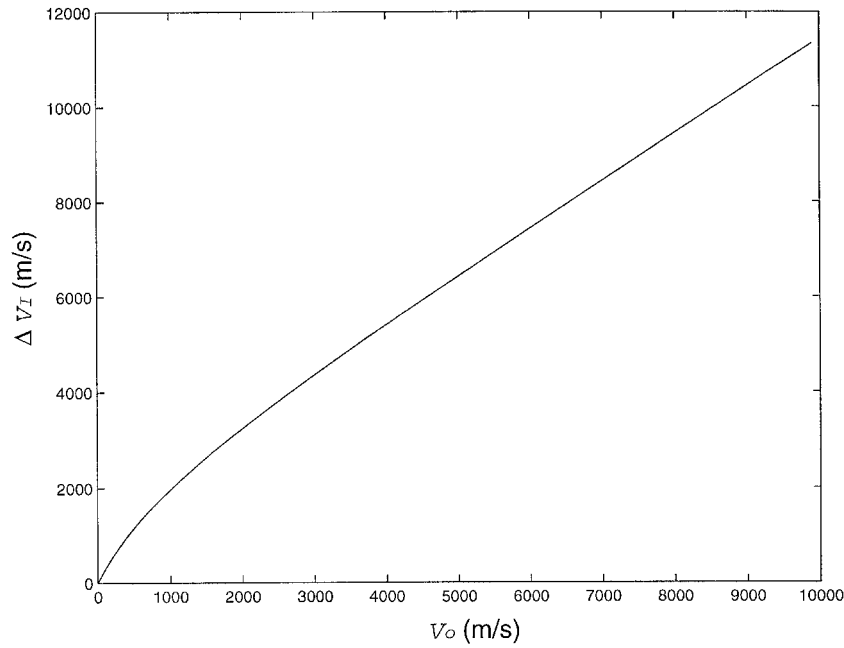

Fig. 3 ΔV_I **vs** V_0 **for** $V_i = 0.$

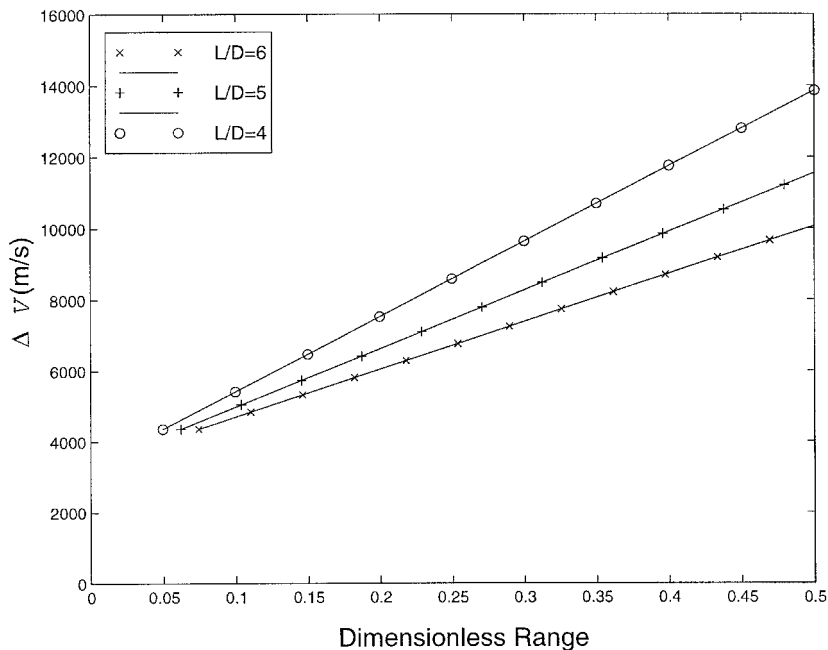**Fig. 4** ΔV_{Total} **vs** ϕ_{Total} **of a PHC trajectory.**

optimal γ_f of 8.42, 6.76, and 5.67 deg for a vehicle with a constant L/D of 4, 5, and 6, respectively. The V_0 for all cases shown is 3000 m/s.

ΔV Performance Comparison of Various Trajectory Types

Using the approximate R_{Total} and ΔV_{Total} expressions developed in the preceding text for periodic hypersonic cruise trajectories, it is now possible to compare the performance of various trajectory types to determine their efficiency in achieving long-range at minimal ΔV expenditure. Trajectory types of interest include PHC, HC, HBG, SUBO, and SUBC.

However, before these trajectory types can be compared against one another, it must be pointed out that the approximate expressions developed earlier for ΔV_{Total} are only a function of vehicle V_0, L/D ratio, γ_f, and the assumed isothermal model of the atmosphere. Issues associated with vehicle heat load, gross takeoff weight, and exact configuration have been neglected for now to simplify the ΔV comparison of trajectory types for achieving long-range.

Assuming that the mission goal is being able to fly halfway around the Earth (approximately 20,000 km), Fig. 5 reveals that the total ΔV required for PHC trajectories is only a function of V_0 and the L/D ratio of the vehicle. Notice that the ΔV performance is improved in general by increasing V_0 and L/D. In addition, in the limit as the boost velocity increases, PHC trajectories become HBG trajectories regardless of the value of the vehicle's L/D ratio. This is because the number of sustaining burns required to achieve the desired range approaches zero as the boost velocity is increased. Thus, all of the range is achieved by simply boosting up to the appropriate velocity and gliding for the remainder of the flight. However, such a

trajectory is not without penalty because high boost velocities at the end of the ascent profile may require better propulsion and structures technology. Also, heating load for long-range glide trajectories will be significant. Therefore, to demonstrate the ΔV performance benefits of PHC trajectories over other types, assumptions will be made about the state of the art in current hypersonic vehicle, aerodynamic, and propulsion technology. This information is summarized in Table 1.

With the mission goal assumed to be a flight halfway around the Earth, Fig. 6 compares the ΔV performance of the five aforementioned trajectory types incorporating the preceding assumptions in hypersonic vehicle technology. Notice that when restrictions are placed on propulsion and structures technology, PHC trajectories have a superior ΔV performance over HC trajectories for long-range. However, HBG and SUBO trajectories achieve better ΔV performance over PHC trajectories, albeit with a significant penalty paid for higher boost velocities. The SUBC trajectory suffers the worst performance except for very short ranges. This result is consistent with the current operation of aircraft today, which are very fuel efficient over short distances.

While the preceding ΔV comparison provides some insight into the efficiency of PHC trajectories over long-range, it does not give a complete picture with regard to the current state of art in vehicle propulsion, aerodynamic, and structures technology. The following sections attempt to bridge this gap by incorporating information about hypersonic vehicle technology.

Range/Mass Efficiency Parameter for Performance Comparisons

The Brequet range equation is commonly used to incorporate the considerations of aerodynamic, propulsion, and struc-

Table 1   Assumptions for performance comparisons

Trajectory type	L/D	V_0 m/s[a]	Comments
Hypersonic			
PHC	4	3000	Higher L/D ratios are possible, but lead to
HC	4	3000	higher g-loads and heating loads.
HBG	4	4000–8000	
SUBO	4	7000–8000	
Subsonic			
SUBC	20	N/A	Cruise speed = 250 m/s

[a] $a_\infty = 300$ m/s.
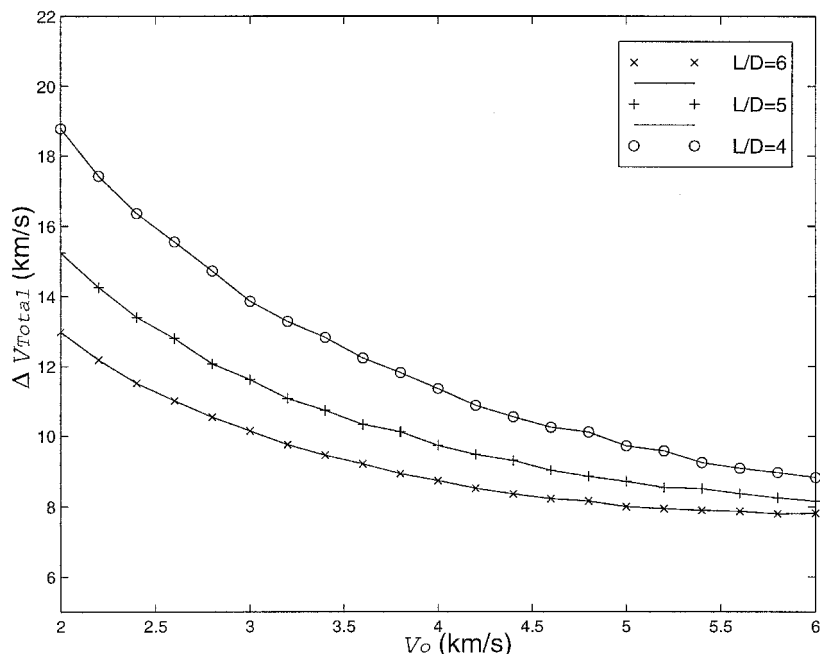

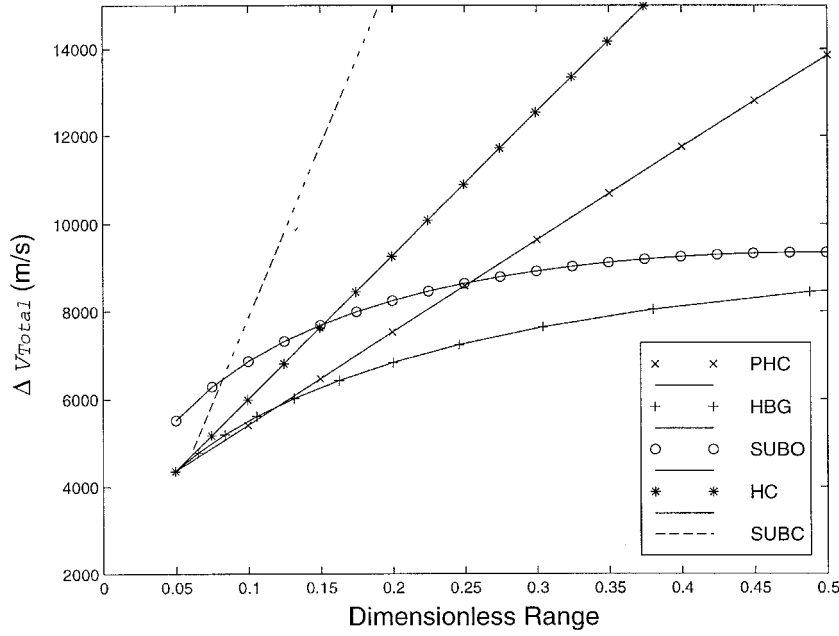Fig. 5 ΔV_{Total} vs V_0 for 20,000-km-range PHC trajectory.

Fig. 6   Comparison of PHC to other trajectory forms.

tures technology into the performance analysis of subsonic, supersonic, and hypersonic cruising aircraft. It is given by

$$R = (L/D)I_{sp}V \ln(m_i/m_f) \qquad (44)$$

where I_{sp} is the specific impulse of the propulsion system, m_i is the mass of the vehicle at takeoff, m_f is the mass of the vehicle upon landing, and V is the cruising velocity.

This relationship can be nondimensionalized by dividing through by 2π and R_e, the radius of the Earth

$$\phi = (L/D)(I_{sp}V/2\pi R_e)\ln(m_i/m_f) \qquad (45)$$

where

$$\phi = R/2\pi R_e \qquad (46)$$

Now by dividing ϕ by $\ln(m_i/m_f)$, a nondimensional mass efficiency parameter, E, can be defined as

$$E = \phi/\ln(m_i/m_f) \qquad (47)$$

This parameter captures, in a single nondimensional number, a measure of performance including both vehicle technology and trajectory performance considerations. For steady-state subsonic, supersonic, or hypersonic cruising flight, E is a constant, given by

$$E = (L/D)(I_{sp}V/2\pi R_e) \qquad (48)$$

The mass term, $\ln(m_i/m_f)$, for PHC, SOBC, and HBG can be calculated using the ideal rocket equation:

$$\ln(m_i/m_f) = \Delta V/I_{sp}g \qquad (49)$$

The rocket equation is valid here because the ΔV derivation assumed impulsive burns. A general form for E can be defined by combining Eqs. (47) and (49):

$$E = RI_{sp}g/2\pi R_e\Delta V \qquad (50)$$

It is assumed that a vehicle flying a PHC trajectory will employ a multicycle engine; therefore, the I_{sp} of the vehicle will vary with Mach number. Figure 7 illustrates the variation
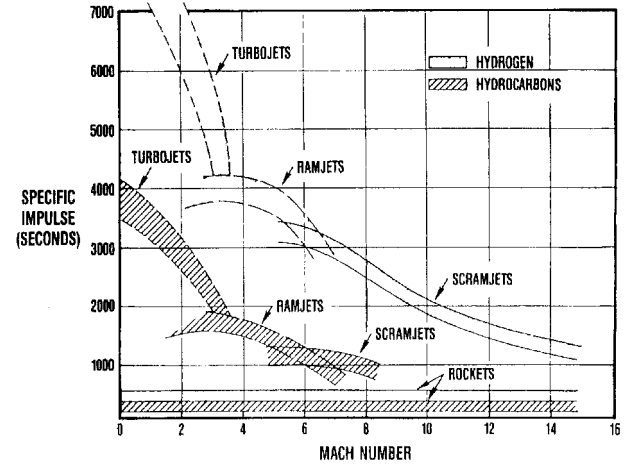

Fig. 7   Variation of I_{sp} with Mach number for various engine technologies.

of I_{sp} with a Mach number that can be expected for various types of propulsion technology.[10] It is unlikely that a single engine will be able to achieve the I_{sp} illustrated in Fig. 7 across the entire range of Mach numbers envisioned for a PHC trajectory. However, based on the current state of the art in propulsion technology, an RBCC engine[11] is a likely candidate for a PHC trajectory. While many types of RBCC engines exist and have widely varying performances, the current study used an ejector ramjet/scramjet rocket engine similar to the aerojet strutjet. Figure 8 is a conservative estimate of the I_{sp} that can be expected from this type of RBCC engine using hydrogen fuel. The engine is in ejector/rocket mode from takeoff to 600 m/s, in ramjet/scramjet mode from 600 to 3600 m/s, and in rocket mode above 3600 m/s. The I_{sp} for ejector/rocket mode has been modeled using the equation

$$I_{sp}(V) = 380 + 2.767V \qquad (51)$$

The ramjet/scramjet mode has been modeled by estimating a curve fit of the technologies presented in Fig. 7:

$$I_{sp}(V) = 6592 \exp(-5.893 \times 10^{-4}V) + 450 \qquad (52)$$

where Mach numbers were replaced with velocity, assuming a constant speed of sound throughout the atmosphere of 300 m/s. Finally, the rocket mode assumed an I_{sp} of 450 s.

To compute the E for PHC, or any other hypersonic trajectory, it is necessary to estimate an I_{sp}^e for the entire flight. The I_{sp}^e during cruise phase is a constant and can be obtained from Fig. 8. For the boost phase, the I_{sp}^e is a function of the ascent trajectory, and the I_{sp} vs Mach number function shown in Fig. 8. Using the rocket equation, I_{sp}^e is defined as

$$I_{sp}^e = \frac{\Delta V_I}{\ln(m_f/m_0)g} \qquad (53)$$

From Eq. (32) and the definition $c = I_{sp}g$

$$\frac{dV}{f(V)} = dV_I = I_{sp}(V)g\frac{dm}{m} \qquad (54)$$

so

$$\frac{dV}{f(V)I_{sp}(V)g} = \frac{dm}{m} \qquad (55)$$

Integrating

$$\ln\left(\frac{m_f}{m_0}\right) = \frac{1}{g}\int_{V_i}^{V_0}\frac{dV}{f(V)I_{sp}(V)} \qquad (56)$$

This relationship can be inserted into Eq. (53) along with the expression for ΔV_I in Eq. (37), to give the following expression for I_{sp}^e during the boost phase:

$$I_{sp}^{e-Boost} = \int_{V_i}^{V_0}\frac{dV}{f(V)}\Big/\int_{V_i}^{V_0}\frac{dV}{f(V)I_{sp}(V)} \qquad (57)$$

A special case of Eq. (57) is when a known amount of ΔV is divided into two or more segments of ΔV_I, which each have
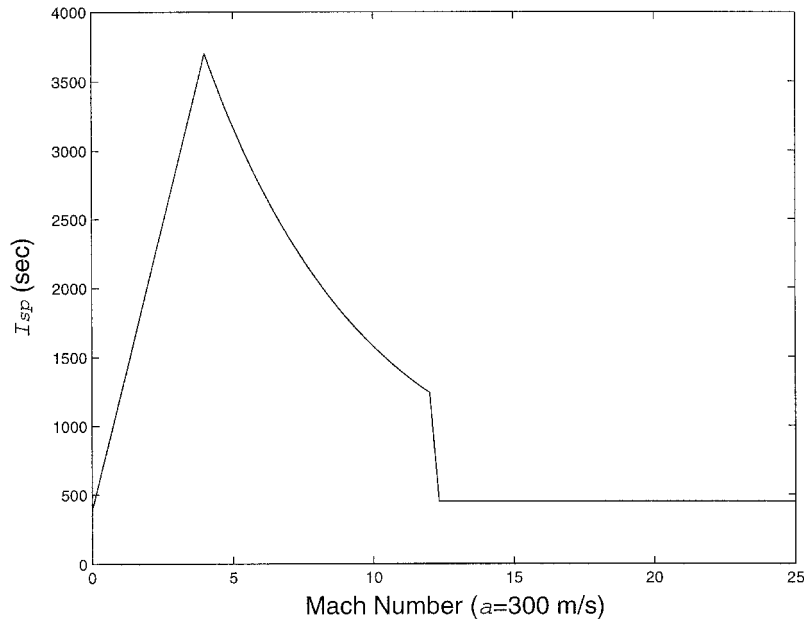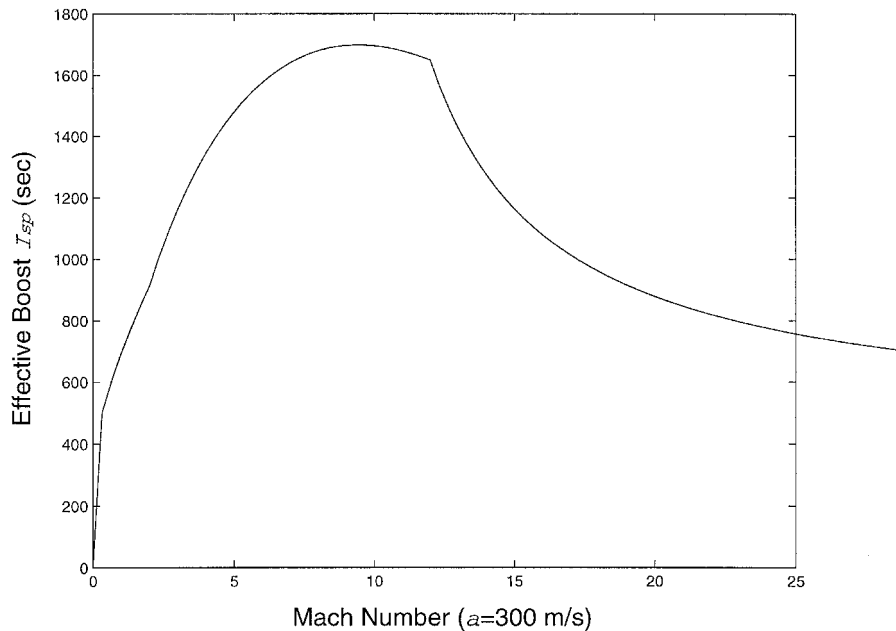

Fig. 8 I_{sp} vs Mach number for RBCC engine.

Fig. 9 $I_{sp}^{e-Boost}$ vs boost Mach number for RBCC engine boosting from takeoff.

known or constant I_{sp}. For this special case, Eq. (57) has the following form:

$$I_{sp}^e = \Delta V_I^{Total} \Big/ \sum_{i=1}^n \frac{\Delta V_I^{Total}}{I_{sp}^i} \qquad (58)$$

Figure 9 shows the $I_{sp}^{e-Boost}$ for a range of boost velocities. In all of the cases presented in this paper, the performance of a hydrogen/oxygen RBCC propulsion system has been assumed. To obtain $I_{sp}^{e-total}$, the following equation can be used:

$$I_{sp}^{e-Total} = \frac{\Delta V_{Total} I_{sp}^{e-Boost} I_{sp}^{e-Cruise}}{\Delta V_{Boost} I_{sp}^{e-Cruise} + \Delta V_{Cruise} I_{sp}^{e-Boost}} \qquad (59)$$

which is an expansion of Eq. (58) for the special case.

The relationships for range and ΔV developed earlier for PHC trajectories are inserted into Eq. (59) to calculate the value of E. Likewise, the common relationships for range and ΔV of other trajectories can be inserted into Eq. (59) to calculate E numbers for comparison. In a comparison of different trajectory types, analytical relationships for range and ΔV are not necessary to calculate an efficiency number. If the performance specifications of an existing aircraft are known, Eq. (48) can be used to calculate the demonstrated E performance of that vehicle. For example, a Boeing 747-400 can fly 13,400 km with a takeoff weight of 394,620 kg and a landing weight of 219,630 kg, which computes to an E of 0.573. This performance measure will serve as the tool for comparing existing aircraft with proposed hypersonic trajectories.
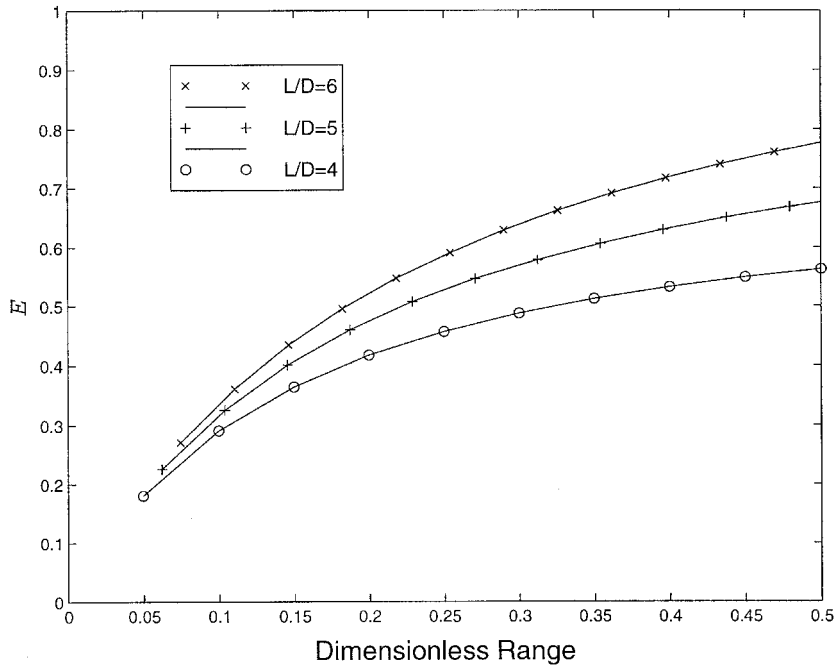

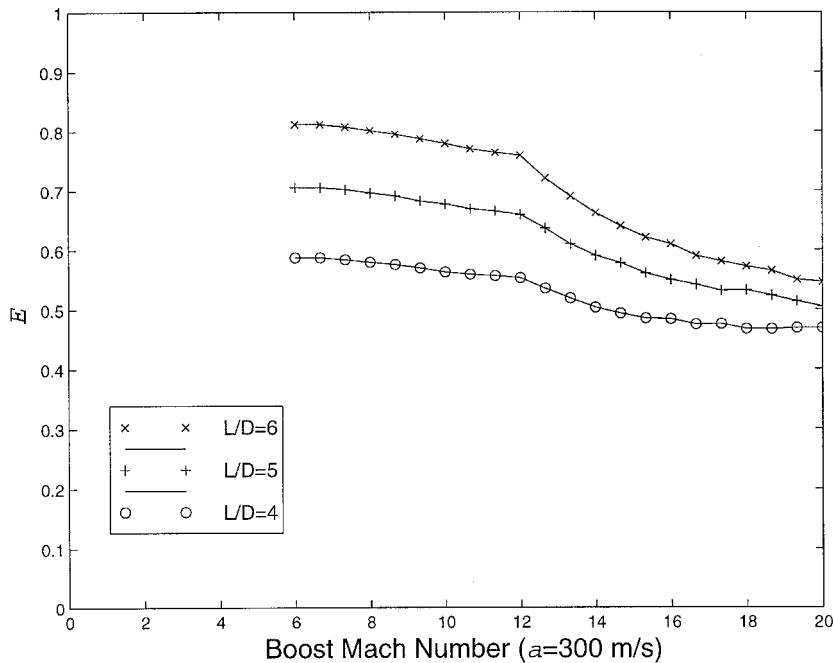Fig. 10   Range/mass efficiency number (E) of PHC trajectories.

Fig. 11   Range/mass efficiency number (E) of PHC trajectory vs boost velocity.

Comparison of Flight Profiles

Figure 10 shows the range/mass efficiency number of PHC trajectories for vehicle L/D of 4, 5, and 6. For all cases shown, a boost velocity of 3000 m/s and a hydrogen RBCC engine are assumed. Figure 11 shows E as a function of the boost velocity and the vehicle L/D for a 20,000-km flight.

As concluded in the previous section, PHC trajectories tend to be more efficient for higher L/D. Although it was not obvious in the previous section, PHC trajectories become less efficient for boost velocities above 3600 m/s. This loss of efficiency results from a decrease in $I_{sp}^{e-\text{total}}$, as the propulsion system is required to operate at velocities above 3600 m/s. This can be clearly seen in Fig. 8, where the RBCC engine operates in its least efficient mode, the rocket mode, above 3600 m/s.

All multicycle engines must transition to rocket mode at some velocity. If the velocity for this transition can be pushed to a higher velocity, the trajectory can be flown more efficiently by boosting to a higher velocity. The efficiency of a PHC trajectory is strongly connected to available propulsion technology.

Figure 12 shows a comparison of PHC trajectories to subsonic, supersonic, and hypersonic cruise. This figure also compares PHC trajectories to HBG and SUBO trajectories, using an L/D of 4 for the PHC, HC, and HBG cases. The boost velocity is 3000 m/s for all hypersonic trajectories. All of the hypersonic trajectories use the propulsion model presented earlier. Results for HBG and SUBO are shown with rockets only and also with an integrated RBCC engine for completeness. It is highly unlikely that a vehicle will fly an HBG or SUBO
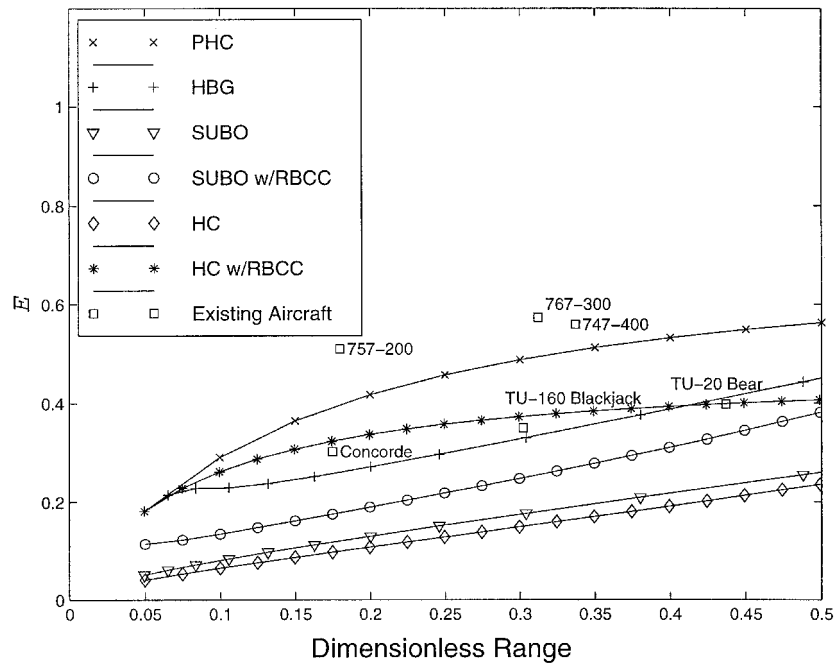

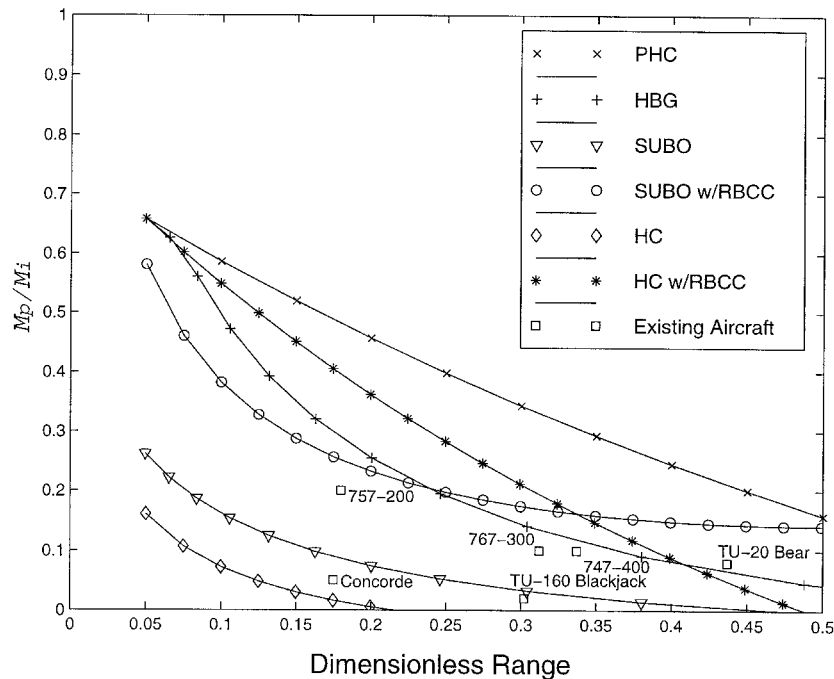Fig. 12   Range/mass efficiency number (E) vs range of various trajectory forms.

Fig. 13   Comparison of payload-carrying capability of vehicles flying various trajectory forms.

trajectory with an RBCC engine because one could not use it again. For subsonic and supersonic cases, data points representing existing aircraft are shown.

Payload Mass Advantage of Vehicles Flying a PHC Trajectory

From the previous section it is clear that a vehicle flying a PHC trajectory is more efficient and, therefore, able to carry more payload across greater distances than other approaches. A vehicle designed to fly at hypersonic speeds has an additional advantage over subsonic and supersonic aircraft, which makes its ability to carry payload even greater. The structural efficiency of a hypersonic vehicle is better than the structural efficiency of an aircraft designed for subsonic or supersonic flight. The configuration of a hypersonic vehicle blends the fuselage and aerodynamic surfaces into one long slender body. The structural elements that hold tankage for fuel, pressure volumes for payload, and support for aerodynamic surfaces are shared throughout the vehicle. This is in contrast to the structural components of subsonic and supersonic aircraft. Most of the structural elements of these vehicles are specialized in their purpose. The fuselage is primarily concerned with containing a pressure volume for payload and crew and typing together the various parts of the aircraft. The wing and tail structures are cantilevered from the fuselage and are specialized toward distributing aerodynamic loads. In terms of structural mass, a hypersonic vehicle configuration is superior. This advantage amplifies the performance superiority of PHC trajectories over existing subsonic and supersonic trajectories. This section will quantify the advantage and make a comparison of the payload capability of vehicles flying different trajectory forms. The accounting of vehicle mass is defined as follows:

$$m_i = m_s + m_{fu} + m_e + m_p \tag{60}$$

where m_i is the initial, or takeoff, mass of the vehicle; m_s is the structural mass of the vehicle, which includes everything except the engines, fuel, and payload; m_{fu} is the fuel mass; m_e is the engine mass; and m_p is the payload mass. Dividing through by m_i and substituting some common mass relationships, an expression for payload fraction can be developed:

$$\left(\frac{m_s}{m_i} + \frac{m_{fu}}{m_i} + \frac{m_e}{m_i}\right) + \frac{m_p}{m_i} = 1 \tag{61}$$

$$\left(\frac{m_s}{m_i} + \frac{m_{fu}}{m_i} + \frac{m_e}{m_i}\right) = \frac{(1 - MR)}{MF} \tag{62}$$

where MR = mass ratio, m_i/m_f = $\exp-(\Delta V/I_{sp}g)$ or $\exp[-(R/R_eE)]$, m_f = final mass of the vehicle, $m_s + m_e + m_p$, and MF = vehicle fuel mass fraction = $m_{fu}/m_{fu} + m_s + m_e$. Using these equations, the payload to takeoff mass ratio can be determined as

$$\frac{m_p}{m_i} = \frac{MR + MF - 1}{MF} \tag{63}$$

Mass fractions for current hypersonic vehicle designs vary from 0.70 to 0.80.[12] This compares to an MF of 0.85–0.95 for single-stage suborbital vehicles. Assuming the more conservative MF values of 0.70 for PHC, HBG with RBCC, and HC trajectories, and 0.85 for SUBO and HBG without RBCC trajectories, Fig. 13 shows the comparison of payload mass to takeoff mass (m_p/m_i) of PHC vehicles to vehicles flying other trajectory forms. Existing subsonic and supersonic vehicles are cited.

These results indicate that a PHC trajectory could have significant performance advantages over traditional hypersonic cruise and suborbital ballistic flight. In addition, it appears that a PHC trajectory has advantages over modern subsonic and supersonic aircraft in terms of range, payload-carrying capability, and higher airspeed.

Summary and Conclusions

The PHC trajectory has been described and analyzed. It has been shown to be superior, in terms of global reach potential and payload performance, in comparison with traditional hypersonic trajectories and even subsonic and supersonic aircraft. Vehicles designed to fly PHC trajectories may be less challenging to construct than previous hypersonic vehicles. PHC trajectory characteristics may have several benefits that enable the use of technology that is currently available in the airframe, propulsion, and thermal-protection fields. A hypersonic vehicle flying a PHC trajectory may be the first implementation of a practical hypersonic vehicle, for global reach.

References

[1]Speyer, J. L., Dannemiller, D., and Walker, D., "Periodic Optimal Cruise of an Atmospheric Vehicle," *Journal of Guidance, Control, and Dynamics*, Vol. 8, No. 1, 1985, pp. 31–38.

[2]Chuang, C.-H., and Speyer, J. L., "Periodic Optimal Hypersonic Scramjet Cruise," *Optimal Control Applications and Methods*, Vol. 8, July–Sept. 1987, pp. 231–242.

[3]Speyer, J. L., "Periodic Optimal Flight," *Journal of Guidance, Control, and Dynamics*, Vol. 19, No. 4, 1996, pp. 745–753.

[4]Chuang, C.-H., and Morimoto, H., "Periodic Optimal Cruise for a Hypersonic Vehicle with Constraints," *Journal of Spacecraft and Rockets*, Vol. 34, No. 2, 1997, pp. 165–171.

[5]Rudd, L., vonEggers, Pines, D. J., and Carter, P. H., "Suboptimal Damped Periodic Cruise Trajectories for Hypersonic Flight," *Journal of Aircraft* (to be published).

[6]Sanger, E., and Brendt, J., "A Rocket Drive for Long Range Bombers," Technical Information Branch, Navy Dept. Translation CGD-32, Aug. 1944.

[7]Eggers, A. J., Allen, J. H., and Neice, S. E., "A Comparative Analysis of the Performance of Long-Range Hypervelocity Vehicles," NACA TR 1382, Dec. 1954.

[8]Wiesel, W. E., *Spaceflight Dynamics*, McGraw–Hill, New York, 1994.

[9]Foster, R., Escher, W., and Robinson, J., "Air Augmented Rocket Propulsion Concepts," Air Force Astronautics Lab., AD-B121 965, April 1988.

[10]Brewer, D. G., *Hydrogen Aircraft Technology*, CRC Press, Boca Raton, FL, 1991.

[11]Billig, F., "The Integration of the Rocket with the Ram-Scramjet as a Viable Transatmospheric Accelerator," International Society for Air Breathing Engines Meeting, Tokyo, 1993.

[12]Takashima, N., Lewis, M. J., Lockwood, M. K., Bogar, T., and Johnson, D., "Waverider Configuration Development for the Dual Fuel Vehicle," AIAA Paper 96-4593, Nov. 1996.